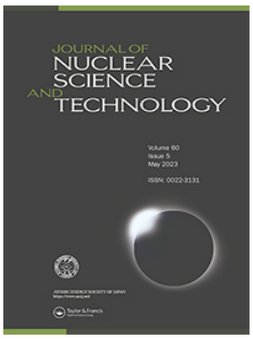

Journal of Nuclear Science and Technology

ISSN: (Print) (Online) Journal homepage: https://www.tandfonline.com/loi/tnst20

^{241}Am Neutron Capture Cross Section in the keV region using Si and Fe-filtered neutron beams

Gerard Rovira, Atsushi Kimura, Shoji Nakamura, Shunsuke Endo, Osamu Iwamoto, Nobuyuki Iwamoto, Tatsuya Katabuchi, Yu Kodama & Hideto Nakano

To cite this article: Gerard Rovira, Atsushi Kimura, Shoji Nakamura, Shunsuke Endo, Osamu Iwamoto, Nobuyuki Iwamoto, Tatsuya Katabuchi, Yu Kodama & Hideto Nakano (2023) ^{241}Am Neutron Capture Cross Section in the keV region using Si and Fe-filtered neutron beams, Journal of Nuclear Science and Technology, 60:5, 489-499, DOI: 10.1080/00223131.2022.2116496

To link to this article: https://doi.org/10.1080/00223131.2022.2116496

Published online: 28 Sep 2022.

JOURNAL OF NUCLEAR SCIENCE AND TECHNOLOGY
2023, VOL. 60, NO. 5, 489–499
https://doi.org/10.1080/00223131.2022.2116496

ARTICLE

^{241}Am Neutron Capture Cross Section in the keV region using Si and Fe-filtered neutron beams

Gerard Rovira[a], Atsushi Kimura[a], Shoji Nakamura[a], Shunsuke Endo[a], Osamu Iwamoto[a], Nobuyuki Iwamoto[a], Tatsuya Katabuchi[b], Yu Kodama[b] and Hideto Nakano[b]

[a]Nuclear Science and Engineering Center, Japan Atomic Energy Agency, Ibaraki, Japan; [b]Laboratory for Zero-Carbon Energy, Institute of Innovative Research, Tokyo Institute of Technology, Tokyo, Japan

ABSTRACT

The neutron capture cross-section of ^{241}Am was measured in the keV neutron range using the recently implemented neutron filtering system of the Accurate Neutron-Nucleus Reaction Measurement Instrument (ANNRI) beamline in the materials and life science (MLF) facility of the Japan Proton Accelerator Research Complex (J-PARC). Filter arrays consisting of 20 cm of ^{nat}Fe and ^{nat}Si were employed in separate measurements to provide filtered neutron beams with averaged neutron energies of 23.5 (Fe), 51.5 and 127.7 (Si) keV. The present ^{241}Am results were obtained relative to the ^{197}Au neutron capture yield by applying the total energy detection principle together with the pulse-height weighting technique. The ^{241}Am neutron capture cross-section was determined as 2.72(29) b at 23.5 keV, 2.14(26) b at 51.5 keV and 1.32(10) b at 127.7 keV with total uncertainties in the range of 8 to 12%, much lower in comparison to the latest time-of-flight experimental data available.

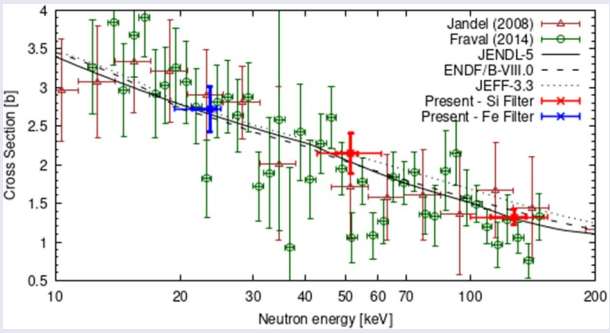

ARTICLE HISTORY
Received: 10 May 2022
Revised: 28 Jul 2022
Accepted: 15 Aug 2022

KEYWORDS
^{241}Am; neutron capture cross-section; J-PARC; ANNRI; MLF; minor actinide; neutron filter

1. Introduction

The advent of partitioning and transmutation (P&T) of high-level radioactive waste (HLW) has allowed for the possibility of the long-lived components of spent nuclear fuel to be re-utilized as energy resources in advanced nuclear reactors systems, while mitigating the long-term environmental impact of such elements [1]. Currently, the Japan Atomic Energy Agency (JAEA) is targeting the transmutation of minor actinides (MAs) through the use of Accelerator-Driven Systems (ADS), a reactor facility that involves the use of a 1.5 GeV-20 μA proton accelerator together with a subcritical reactor. The principle of the nuclear transmutation of MAs using ADS has been recently proven at the Kyoto University Critical Assembly (KUCA) in the work of Pyeon *et al.* [2]. The ADS design at JAEA is meant to consist of a lead-bismuth eutectic (LBE) cooled 800 MW thermal power reactor with the capacity to transmute about 250 kg per 300 effective full power days (EFPDs), equal to the total amount of MAs produced by 10 Pressurized Water Reactors (PWR) per year [3,4]. The latest revised version of the ADS will include ^{241}Am with an MA isotopic concentration of 35%, second only to ^{237}Np (50%), with an upper limitation for the reactivity coefficient k_{eff} set to 0.98 [5]. The uncertainty of the k_{eff} is tied to uncertainty of the nuclear data used in calculation designs. The uncertainty contribution to the k_{eff} by the JENDL-4.0 [6] nuclear data was quantified in the recent works of Iwamoto et al [7,8] with the uncertainty related to the ^{241}Am neutron capture cross-section being the main contributor among all MAs at the neutron energy range from 0.454 keV to 1.35 MeV. In this energy range, evaluated nuclear data in JENDL-5 [9] for the neutron capture cross-section of ^{241}Am includes similar uncertainties to those in JENDL-4.0, ranging from 3% to as high as 40%, that stem from the experimental data available. In order to

CONTACT Gerard Rovira gerard.rovira@jaea.go.jp Nuclear Science and Engineering Center, Japan Atomic Energy Agency, Ibaraki, Japan

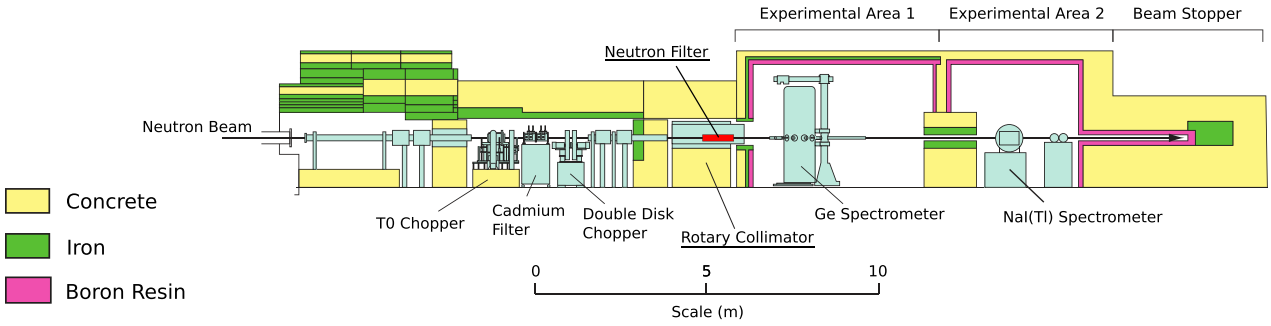

Figure 1. Schematic view of the and ANNRI beamline.

resolve the uncertainties introduced by the evaluated nuclear data, ADS test facilities are planned to be constructed. Nonetheless, with no set date for such facilities to be operational, the need for further accurate experimental results becomes much higher.

In terms of the experimental data in the keV region, the latest relevant experimental data in the keV region include the time-of-flight (TOF) works of Fraval *et al.* [10] and Jandel *et al.* [11], which show discrepancies among them from 5% to 30% with total uncertainty values higher than 15% above 10 keV. One of the reasons for this is that ^{241}Am is highly radioactive due to its relatively short half-life (^{241}Am $t_{1/2}$ = 432.2 yr) compared to other MAs (^{237}Np $t_{1/2}$ = 6.6 M yr). This fact, together with the low neutron capture cross-section in the keV region, makes the measurement of the neutron capture cross-section of ^{241}Am extremely susceptible to the influence of both sample-dependent, which includes decay and neutron elastic-scattered backgrounds and sample-independent backgrounds.

In the present work, the neutron capture cross-section of ^{241}Am was measured at the Accurate Neutron-Neutron Reaction Measurement Instrument (ANNRI) using the neutron filtering technique. ^{nat}Si and ^{nat}Fe were employed as filter materials to tailor quasi-monoenergetic neutron beams with average incident neutron energies of 51.5 and 127.7 keV (Si) and 23.5 keV (Fe). The present study intends to provide experimental evidence of the ^{241}Am neutron capture cross-section, with lower uncertainties than those present in the current experimental data available, for the design ADS facilities. An explanation of the experimental setup and the neutron filtering technique is given in section 2, followed by a description of the data reduction process in section 3. The cross-section results are presented and discussed in section 4 with the conclusions provided in section 5.

2. Experimental setup

2.1. Neutron filtering system

The experimental work was conducted at the ANNRI beamline of the materials and life science (MLF) experimental facility in the Japan Proton Accelerator Research Complex (J-PARC) using the highly intense pulsed neutron beam provided by the Japanese Spallation Neutron Source (JSNS) of J-PARC. However, the J-PARC accelerator is currently operated in double-bunch mode, where two proton bunches with a time difference of 0.6 μs are shot to the JSNS in order to generate pulsed neutrons at a repetition rate of 25 Hz, making fast-neutron timing experiments unattainable without a high degree of ambiguities. Hence, in order to bypass these ambiguities and perform accurate neutron capture cross-section measurements, the newly implemented neutron filtering system in the ANNRI beamline was employed in the present experiments in conjunction with the NaI(Tl) spectrometer. The experiments were performed with filter configurations of 20 cm of ^{nat}Si and ^{nat}Fe in separate measurements in order to mold the double-bunch incident neutron flux into quasi mono-energetic neutron beams with averaged energies of 51.5 and 127.7 keV (Si) and 23.5 keV (Fe). The filter materials were introduced into the rotary collimator of the ANNRI beamline, upstream of the experimental areas as shown in Figure 1. Moreover, a thick cadmium filter was also employed in all measurements to prevent thermal neutrons from activating the filter materials. Capture γ-rays were detected using the NaI(Tl) spectrometer in ANNRI beamline situated at a flight path of 27.9 m with respect to the JSNS moderator surface. A CAEN V1720 time digitizer [12] was employed to determine the neutron TOF as the time difference between a trigger signal from the proton beam monitor, for each spallation reaction, and sequential stopping events, i.e. detected prompt γ-rays. Simultaneously, the energy of the detected γ-ray was recorded as the total area readout of the anode signal. The characteristics and performance of the neutron filtering system using the NaI(Tl) spectrometer have already been described in more detail in Ref [13,14]. At the same time, the first neutron capture cross-section results of MAs using the neutron filtering system have already been published in the measurement of ^{243}Am using the Fe filter of Kodama *et al.* [15].

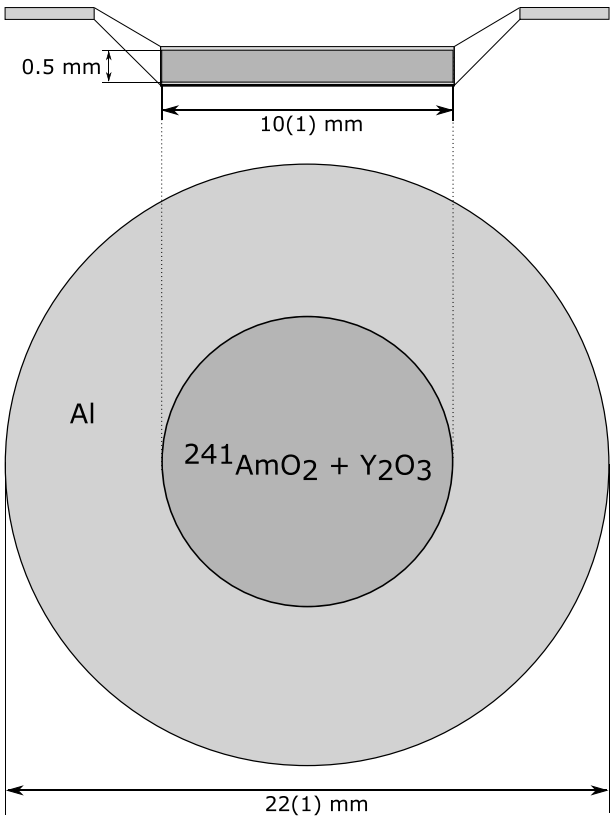

Figure 2. Diagram of the ^{241}Am sample. ^{241}Am oxide is encapsulated in an Al case using Y_2O_3 as binder.

Table 1. Summary of the measurement times.

	Si Filter	Fe Filter	No Filter
^{241}Am	40 h	24 h	16 h
^{197}Au	24 h	8 h	2 h
Dummy	36 h	24 h	16 h
Carbon	24 h	24 h	7 h
Boron	8 h	8 h	5 h
Blank	22 h	18 h	17 h

2.2. Samples and measurements

A pellet of 7.47(10) mg of ^{241}Am oxide enclosed in an Al casing with 46.0 mg of Y_2O_3 used as binder was measured in the present experiments. The mass of ^{241}Am in the sample was deduced from the accurate activity measurement of 957 MBq from the past works of Terada *et al* [16] and Harada *et al* [17] and accounting from the change in activity due to the decay of ^{241}Am. The pellet measured 10.0(1) mm in diameter with an active thickness of 0.50(5) mm. Impurities in the form of ^{237}Np and ^{242}Pu were found in a thorough analysis of the resolved resonance region that amounted to 1.52(3)% and 0.49(8)%, respectively. The sample was encapsulated in an Al case with 0.1-mm-thick walls and an outer diameter of 22.0(1) mm. The layout of the ^{241}Am sample can be seen in Figure 2.

The sample-dependent background relative to the Al canning was estimating by measuring a duplicate of the Al dummy casing without any ^{241}Am oxide included in the sample. Nonetheless, the dummy sample comprised a slightly higher amount of Y_2O_3 in order to guarantee the homogeneity within the dummy case. This mass difference was estimated by means of the 2.59 keV resonance of the ^{89}Y(n,γ) in measurements without any neutron filter. In the present analysis, the ^{241}Am neutron capture cross-section was derived relative to the ^{197}Au cross-section. Thus, a ^{197}Au sample having a diameter of 10.0(1) mm a thickness of 0.100(1) mm and a mass of 153.9 mg was employed to derive the Au neutron capture yield. Moreover, the time distribution of the incident-filtered neutron flux was derived in a measurement of a boron sample with a 90.4% ^{10}B enrichment and a mass of 86.1 mg. This is a commonly used technique since the ^{10}B(n,$\alpha\gamma$)^{7}Li reaction has been extensively measured in the past and, hence, evaluated data for this reaction are deemed highly reliable. Moreover, since the ^{10}B(n,$\alpha\gamma$)^{7}Li reaction emits a sole γ-ray with the energy of 478 keV, events from this reaction can be easily isolated to increase the signal-to-noise ratio. Alongside these samples, a carbon sample with a diameter of 10.0(1) mm, a thickness of 0.50(5) mm and a mass of 73.1 mg was utilized to derive the sample-dependent background related to neutrons scattered at the sample materials, since the elastic scattering cross-section is the dominant reaction channel and it presents a flat energy dependence. Finally, the sample-independent background was estimated in a "blank" measurement with no sample. These samples were measured using both neutron filters, and also in the no neutron filter condition in order to accurately determine the influence of the sample-dependent backgrounds and impurities. The measurement times in the present experiment for each sample are shown in Table 1.

3. Data analysis

The ^{241}Am neutron capture cross-section was determined at the averaged neutron energies 23.5 keV (Fe) and 51.5 and 127.7 keV (Si) relative to the ^{197}Au neutron capture yield in offline analysis. The experimental results were stored successively in two-dimensional list data files with the detected γ-ray energy and the neutron TOF.

3.1. Filtered neutron beams

In the present study, the time distribution of the incident neutron flux was determined using the 90.4%-enriched boron sample measurement by gating the lone 478-keV γ-rays emitted from the ^{10}B(n,$\alpha\gamma$)^{7}Li reaction. The ^{10}B-$\alpha\gamma$ yield, obtained after subtracting the sample-dependent background using the carbon sample measurement and sample-independent

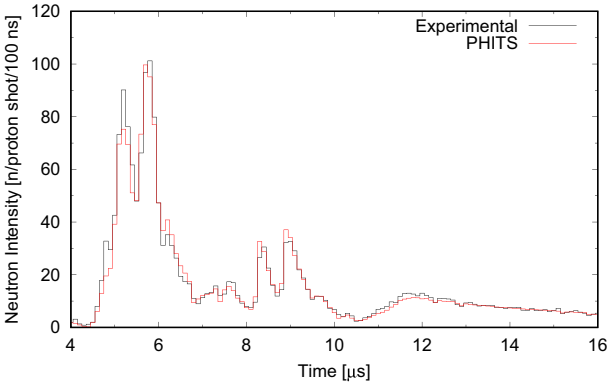

Figure 3. Present filtered neutron flux with 20 cm of ^{nat}Si measured with the boron sample (black) in the present experiment compared to simulations with PHITS.

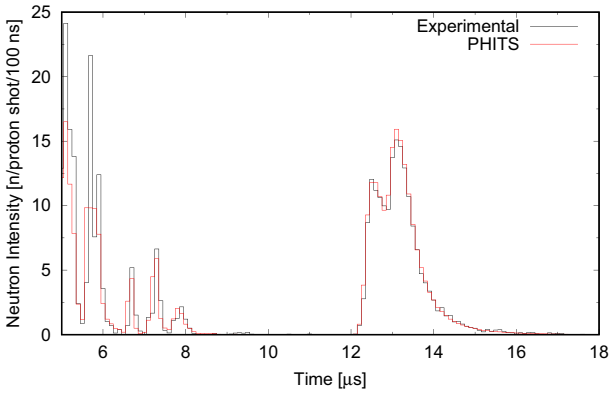

Figure 4. Present filtered neutron flux with 20 cm of ^{nat}Fe measured with the boron sample (black) in the present experiment compared to simulations with PHITS.

background, was divided by the reaction rate calculated in simulations with the PHITS code [18] to remove the energy-dependent influence of the ^{10}B (n,$\alpha\gamma$)^{7}Li reaction. The present time distribution of the incident neutron time distribution filtered with filter configurations of 20 cm of ^{nat}Si and ^{nat}Fe are shown in Figures 3 and 4, respectively. The present results are in concordance with the simulation results using the PHITS code from the previous validation work for the neutron filtering system in ANNRI [13] with similar integration TOF gates from 5 to 6 μs and 8.2 to 9.4 μs for the 127.7 and the 51.5 keV filtered peaks with the Si filter array; and from 12.2 to 14.6 μs for the 23.5 keV peak with the Fe filter configuration. Although the final ^{241}Am cross-section results are determined relative to the neutron capture yield, it is still necessary to accurately determine the time distribution of the incident filtered neutron flux to ensure the correct filtering performance of the neutron filtering system. Moreover, in the present study, the ^{197}Au neutron capture cross-section was also derived relative to the boron sample measurement as means to validate the accuracy of the ^{197}Au neutron capture yield and assess the reliability of the final results.

3.2. Pulse-height weighting technique

The total energy detection principle was applied in the present experiment in order to accurately determine the neutron capture yield for both ^{241}Am and ^{197}Au. For this methodology to be applied, the following premises have to be fulfilled by the detector setup: (1) the detection efficiency is proportional to the γ-ray energy and (2) the detection efficiency is low enough so that only one γ-ray is detected from each deexcitation cascade following a capture event. So as to accomplish that the pulse-height weighting technique (PHWT) [19,20] was applied by means of two distinct weighting functions based on the different characteristics of both the ^{241}Am and ^{197}Au samples. These weighting functions, which were calculated from Monte-Carlo simulations with the γ-ray simulation code SG [21], obey the following:

$$\sum_{I} W(I)R(I,E) = E. \tag{1}$$

with $R(I,E)$ as the response function for the present detector system, including the influence of the sample characteristics, for a γ-ray with energy E detected in the I-th channel and E as the detected γ-ray true energy value. Additionally, in the present setup, the weighting functions were applied with a minimum energy threshold of 600 keV as a means to diminishing the background influence of the 478-keV and 511-keV γ-rays emitted by ancillary materials and the decay γ-rays from ^{241}Am. A comparison of the weighting functions for the ^{241}Am and ^{197}Au samples is shown in Figure 5 which take the form:

$$W(I)_{Am} = 2.2389 \times 10^{1}\sqrt{I} - 5.3171 \times I + 7.8757 \times 10^{-1} I^{3/2} \tag{2}$$

$$- 4.0274 \times 10^{-2} I^{2} + 7.4636 \times 10^{-4} I^{5/2}$$

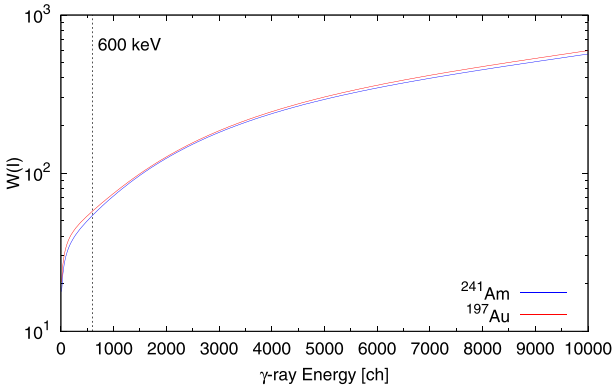

Figure 5. Comparison of the weighting function $W(I)$ for the ^{241}Am (blue) and ^{197}Au (red) samples. These weighting functions were applied to detected events with energy higher than 600 keV.

$$W(I)_{Au} = 2.5982 \times 10^{1}\sqrt{I} - 6.3155 \times I + 8.9017 \times 10^{-1} I^{3/2} - 4.4444 \times 10^{-2} I^{2} + 8.0972 \times 10^{-4} I^{5/2} \quad (3)$$

with I as the detected energy in the detector in channels with a bin width of 25 keV.

Finally, the neutron capture yield for each isotope, Y, can then be determined by means of each respective weighting function as:

$$Y = \frac{\sum_I W(I)S(I)}{B_n + E_n} \quad (4)$$

being $S(I)$ as the detected pulse height spectrum for each channel I. With B_n and E_n as the compound nucleus binding energy and the incident neutron energy, respectively, for both ^{241}Am and ^{197}Au.

3.3. Background subtraction

The detected prompt γ-rays emitted in neutron induced capture events in both the ^{241}Am and ^{197}Au samples have to be isolated from the events caused by other sources, both sample-dependent and sample-independent, as they are recorded together and cannot be separated in online analysis. Thus, several other measurement were performed to isolate and precisely quantify these background layers. The background levels relate to the sample-independent background, estimated in a "blank" measurement with no sample, and the sample-dependent backgrounds, namely, the background events caused by neutrons scattered at the sample and by the casing material, with the latter being only for the ^{241}Am sample. A comparison of the raw detected events for each sample and in the different filter configuration is displayed in Figures 6 and 7.

In addition, since the present experiments were performed using a thick cadmium filter to avoid the activation of the filter materials by thermal neutrons, no neutrons are able to reach the sample position with energies lower than 0.5 eV. Hence, the constant background level for each sample measurement was estimated using the detected events with detected time-of-flight (t) as $5 < t < 35$ ms as can be seen in Figure 8. This is important in the measurement of the ^{241}Am sample to accurately estimate the background events induced by the decay of ^{241}Am.

After subtracting the constant background in all sample measurements, the sample-independent background layer was removed using the "blank" sample measurement with no sample. The net capture yield for both ^{241}Am and ^{197}Au was then obtained by subtracting the sample-dependent background.

As regards to the ^{241}Am sample, the sample-dependent background component was constituted by events caused from (1) the neutrons interacting with both the Al casing material and the Yttrium binder; and by (2) the neutrons scattered at the ^{241}Am sample. The measurement of the dummy case was employed to estimate and subtract the first component of the sample-dependent background, after correcting for the difference in Yttrium mass using the 2.59 keV resonance peak from the ^{89}Y neutron capture reaction. This resonance was clearly visible in a measurement without any filter configuration present. Subsequently, the carbon sample measurement was employed to subtract the background caused to neutrons

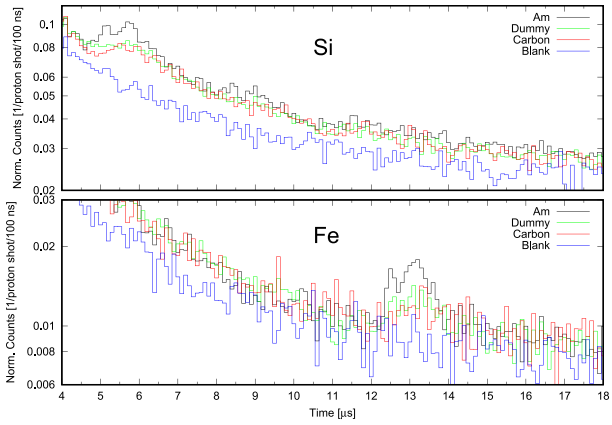

Figure 6. Raw detected events in the Am (black), dummy (green), carbon (red), and blank (blue) measurements for the Si (top) and Fe (bottom) filter configurations. The data from dummy and carbon have not been corrected yet for the difference in yttrium mass; and neutron elastic scattering cross-section and number of atoms, respectively.

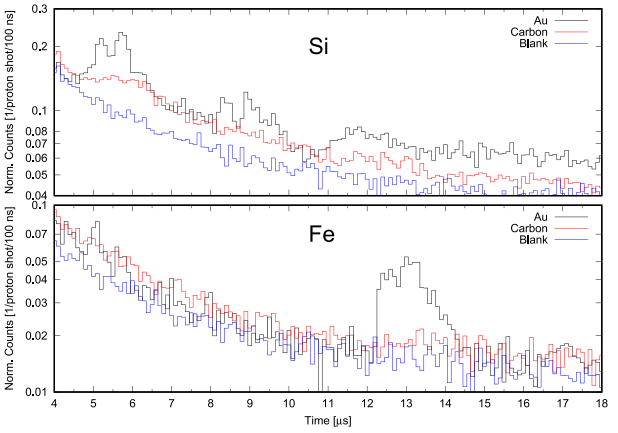

Figure 7. Raw detected events in the Au (black), carbon (red) and blank (blue) measurements for the Si (top) and Fe (bottom) filter configurations. The data from carbon have not been corrected yet for the difference neutron elastic scattering cross-section and number of atoms.

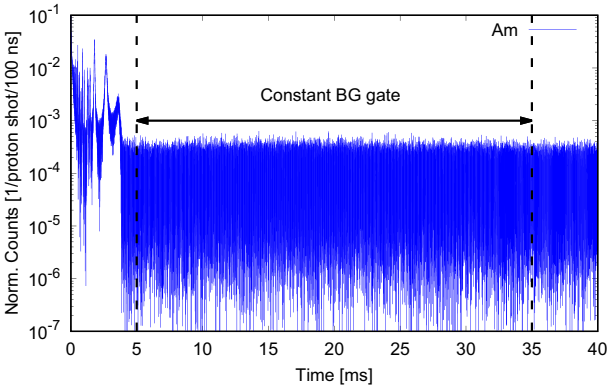

Figure 8. Raw detected events in the Am sample measurements using the Si filter array. The constant background that includes the influence of decay γ-rays was estimated using the flat TOF region from 5 to 35 ms.

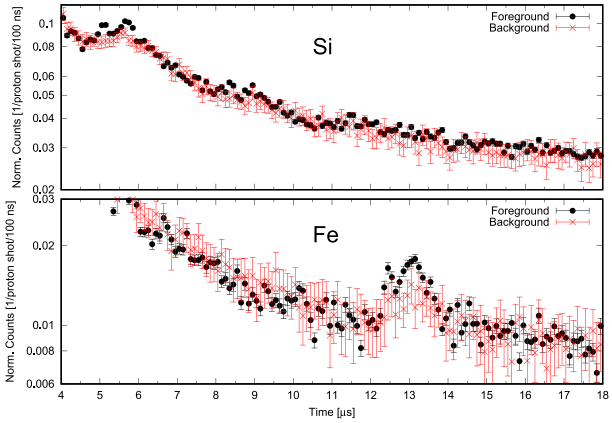

Figure 9. ^{241}Am sample foreground (black) and background (red) events in the Si (top) and Fe (bottom) filters experiments.

scattered at the ^{241}Am atoms. Moreover, since background induced by the case was normalized to the difference in Yttrium mass, the results of the measurement were also utilized to correct for the underestimation of the Al casing background. This process can be summarized by the following:

$$Y_{Am}(E_n) = Y'_{Am}(E_n) - N_{mass} \cdot Y_D(E_n) \qquad (5)$$

$$- Y_C(E_n)\left[\frac{\sigma^{ela}_{Am}(E_n)\frac{m_{Am}}{M_{Am}}}{\sigma^{ela}_{C}(E_n)\frac{m_C}{M_C}} + (1 - N_{mass}) \cdot \frac{\sigma^{ela}_{Al}(E_n)\frac{m_{Al}}{M_{Al}}}{\sigma^{ela}_{C}(E_n)\frac{m_C}{M_C}}\right]$$

with Y_{Am} as the ^{241}Am neutron capture yield. $Y'_{Am}(E_n)$, $Y_D(E_n)$ and $Y_C(E_n)$ stand for the weighted TOF spectrum from the ^{241}Am sample (after the dummy background subtraction), the dummy and the carbon sample, respectively. $\sigma^{ela}(E_n)$, M and m are the neutron elastic scattering cross-section, the atomic mass and the sample mass for ^{241}Am, Al, and carbon. N_{mass} means the normalization factor relative to the Yttrium mass correction. For the case of the ^{197}Au sample, the sample-dependent background is only composed by the neutron elastic scattering background and was estimated using the carbon sample measurement analogously to the ^{241}Am sample.

The weighted TOF foreground and background events normalized in each filter configuration for both the ^{241}Am and ^{197}Au samples are shown in Figures 9 and 10.

Additionally, the accurate estimation of the background levels for both samples can be seen in the pulse-height for the gated foreground and background events at the 127.7 keV filtered peak from 5 to 6 μs for the ^{241}Am and ^{197}Au samples (see Figure 11). The background estimation was able to precisely reproduce the peak at around 6.7 MeV caused by the ^{127}I included in the detector setup.

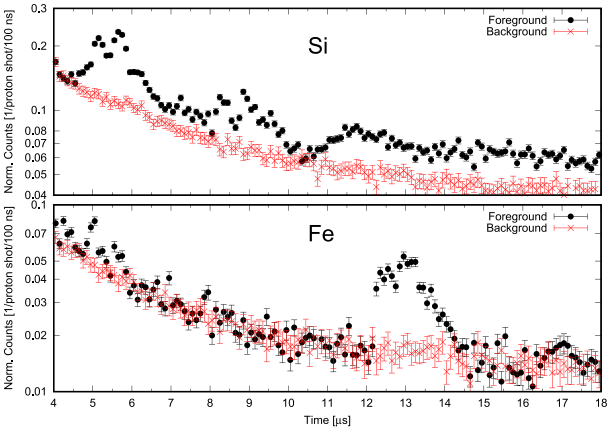

Figure 10. ^{197}Au sample foreground (black) and background (red) events for the Si (top) and Fe (bottom) filters measurements.

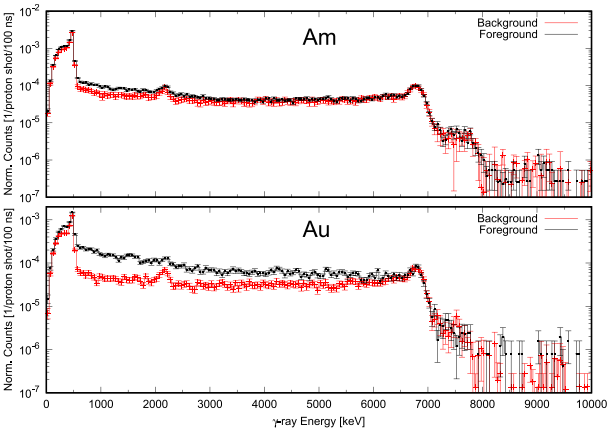

Figure 11. Foreground (black) and background (red) events for the Am (top) and Au (bottom) samples for events gated from 5 to 6 μs (127.7 keV) using the Si filter array.

3.4. Correction for self-shielding, multiple scattering, and fission

Monte-Carlo simulations with the PHITS code [18] were employed to estimate and correct for the effects related to the neutron flux attenuation within the sample, i.e. neutron self-shielding, and for the secondary captures of neutrons after suffering a first elastic interaction with the sample material, namely, multiple scattering effect. These effects were determined as the ratio between the JENDL-5 neutron capture cross-section value and the simulated cross-section results, at the centroid energy point for the three measured filtered beams of 23.5 keV (Fe); and 51.5 and 127.7 keV (Si). Moreover, for the case of ^{241}Am, the influence of fission events has to be taken into account as well. In the present analysis, a correction similar to that of Terada *et al.* [16] was applied using the evaluated data from JENDL-5 for the neutron capture and fission cross-sections of ^{241}Am as follows:

$$C_{fis} = \frac{\sigma_{cap}}{\sigma_{cap} + \sigma_{fis} \cdot \frac{M_{\gamma,fis}}{M_{\gamma,cap}}} \tag{6}$$

where σ_{cap} and σ_{fis} stand for the ^{241}Am capture and fission cross-section taken from JENDL-5, respectively; while $M_{\gamma,cap}$ and $M_{\gamma,fis}$ mean the γ-ray multiplicity emission for the capture and fission reactions. The fission multiplicity value was assumed to be the same as in the work of Verbeke *et al.* [22], with an average value of 7. In the case for the capture reaction, a value of 3.5 following the work of Terada *et al.* was employed. The final correction factors for the ^{241}Am and ^{197}Au are summarized in Tables 2 and 3.

3.5. Cross-section calculation

The neutron capture cross-section of ^{241}Am was determined relative to the ^{197}Au capture yield at the energies of 23.5 (Fe), 51.5 and 127.7 (Si) keV as follows:

$$\sigma_{Am}(E_{n,x}) = \frac{Y_{Am}(E_{n,x})C_{Am}(E_{n,x})C_{fis}(E_{n,x})}{Y_{Au}(E_{n,x})C_{Au}(E_{n,x})} \cdot \frac{S_{Au}}{S_{Am}} \cdot \frac{P_{Au}}{P_{Am}} \cdot \frac{\sigma_{Au}(E_{n,x})}{C_{Ythres}} \tag{7}$$

Table 2. Summary of the self-shielding and multiple scattering correction factors.

	Centroid Energy		
	23.5 keV	51.5 keV	127.7 keV
^{241}Am	0.992(6)	1.010(9)	1.008(9)
^{197}Au	0.990(6)	1.005(7)	1.006(8)

Table 3. Summary of the fission correction factors.

	Centroid Energy		
	23.5 keV	51.5 keV	127.7 keV
^{241}Am	0.988(8)	0.985(7)	0.972(7)

being $Y_{Am}(E_{n,x})$ the ^{241}Am neutron capture yield at for each of the three filtered neutron beams (x); $C(E_{n,x})$ and $C_{fis}(E_{n,x})$ stand for the corrections for self-shielding and multiple scattering; and for the fission events, respectively. S_y and P_y mean the sample area density in "at/b" and the number of proton shots in the measurements, respectively, for the ^{241}Am and ^{197}Au samples. With $\sigma_{Au}(E_{n,x})$ as the JENDL-5 cross-section for Au at the three filtered neutron energies (x) and C_{Ythres} as the correction for yield loss under the 600 keV detection threshold. This last parameter was calculated using theoretical calculations with the CCONE code [23] as the total yield loss under the 600 keV threshold of ^{241}Am relative to that of ^{197}Au as their neutron binding energies are different. This correction factor takes the form:

$$C_{Ythres} = \frac{1 - \frac{\sum_{i=0}^{600} E_{Am(i)}}{B_n^{Am}+E_n} \Big/ \frac{\sum_{i=0}^{\infty} E_{Am(i)}}{B_n^{Am}+E_n}}{1 - \frac{\sum_{i=0}^{600} E_{Au(i)}}{B_n^{Au}+E_n} \Big/ \frac{\sum_{i=0}^{\infty} E_{Au(i)}}{B_n^{Au}+E_n}} \tag{8}$$

where $\sum_{i=0}^{600} E_{Am(i)}$ and $\sum_{i=0}^{\infty} E_{Am(i)}$ mean the energy sum of the capture γ-rays emitted with energies from 0 to 600 keV and of the total emitted, respectively. B_n^{Au} and B_n^{Am} are the binding energies for ^{198}Au and ^{242}Am; with E_n as the filtered neutron energy. In the present analysis, the same correction factor was obtained for each of the three filtered neutron beams, since the difference in averaged neutron energies between the filtered peaks is insignificant in comparison with the binding energies, that amounted to 0.986(4). Further information about this technique is provided in Ref [24].

3.6. Uncertainty analysis

Alongside the statistical uncertainty related to the number of detected events, the systematic uncertainties considered in the present analysis include uncertainties relative to the detector deadtime, the correction factor for self-shielding, multiple scattering and fission; the correction for yield loss under threshold, weighting function calculation; and the ^{241}Am and ^{197}Au samples area density have been considered together with the statistical uncertainty. The uncertainties related to the deadtime correction were estimated as the square root of the corrected counts at each energy point. Area density uncertainties of 1.7% and 1% for the ^{241}Am and ^{197}Au samples, respectively, were assumed from the uncertainties of 0.1 mg for the sample mass and 0.1 mm for the sample diameter. The uncertainty introduced correction factor was estimated assuming total nuclear data uncertainties of 10% and the samples area density uncertainties. Nonetheless, since the correction factors were very close to the unity, the uncertainty introduced by these concept became rather small. 20% uncertainties

were assumed for both calculations with the CCONE code [23,], for ^{241}Am and ^{197}Au that is, with the total uncertainty introduced by the yield loss correction being the quadratic sum of these uncertainties (28%) was multiplied by the yield loss correction of 1.4% to a total of 0.4%. Uncertainty values of 1% were assumed for the determination of both weighting functions. Finally, uncertainties of 2% were assumed for the JENDL-5 ^{197}Au neutron capture cross-section used to determine the present cross-section results. These uncertainties were taken from the IAEA Standard library [25] since JENDL-5 does not include uncertainties for the ^{197}Au neutron capture cross-section. An outline of the systematic uncertainties considered in the present analysis is included in Table 4, followed by the summary of the total uncertainties, including the statistical uncertainties, in Table 5. As displayed in Table 5, the main uncertainty component is the statistical uncertainty in the ^{241}Am sample measurement owing to the mass of ^{241}Am. This made the foreground to background ratio quite tiny as shown in Figure 9

Table 4. Outline of the systematic uncertainties.

Uncertainties	[%]
Deadtime	< 0.1
Correction factor	0.3
Correction under threshold	0.4
Weighting function	
^{241}Am	1.0
^{197}Au	1.0
Area density	
^{241}Am	1.7
^{197}Au	1.0
^{197}Au nuclear data uncertainty	2.0
Total systematic uncertainty	3.2

Table 5. Summary of the total uncertainties.

	Centroid Energy		
	23.5 keV	51.5 keV	127.7 keV
Systematic	3.2%	3.2%	3.2%
Statistical			
^{241}Am	9.7%	11.2%	6.8%
^{197}Au	3.3%	3.3%	2.0%
Total uncertainty	10.8%	12.1%	7.8%

4. Results and discussion

The ^{241}Am neutron capture cross-section was determined at the averaged neutron energies of 23.5, 51.5, and 127.7 keV using the neutron filtering system implemented in the ANNRI beamline by integrating the ^{241}Am neutron capture yield from 12.2 to 14.6 μs when using the Fe filter array; and from 8.2 to 9.4 μs and from 5 to 6 μs with the Si filter assembly, respectively. The present cross-section results were obtained relative to the ^{197}Au neutron capture yield obtained using the same integration gates by means of the pulse-height weighting technique. The ^{241}Am neutron capture cross-section was measured to be 2.72(29) b at 23.5 keV, 2.14(26) b at 51.5 keV and 1.32(10) b at 127.7 keV. The present results are compared to the TOF experimental results of Jandel *et al.* [11] and Fraval *et al.* [10] together with the evaluated data from the JENDL-5 [9], ENDF/B-VIII.0 [26] and JEFF-3.3 [27] nuclear data libraries in Figures 12 and Figure 13 and are summarized in Table 6. Since the neutron energy distribution is not uniform within the filtered peaks, the one-sigma (thick) and two-sigma neutron (thin) neutron energy distributions are displayed as the x-axis bars. Nonetheless, in the present analysis, all the neutrons within the filtered peaks have

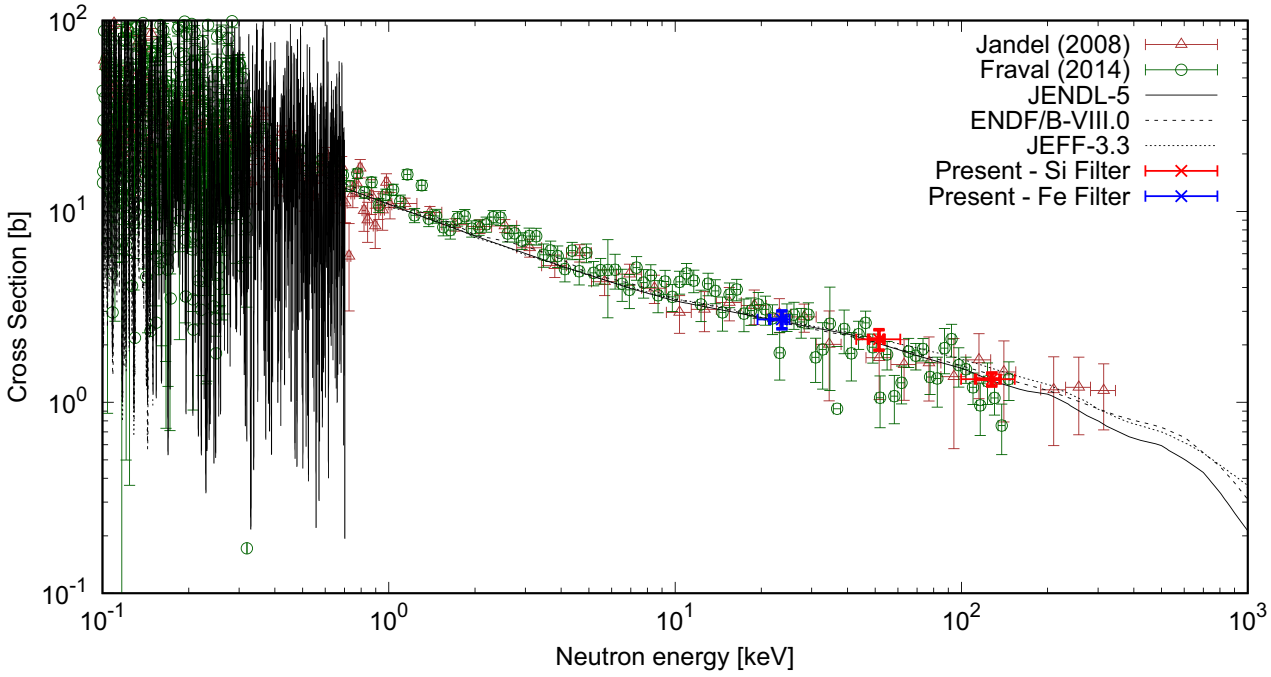

Figure 12. Neutron capture cross-section results for ^{241}Am compared to the latest experimental data and evaluated nuclear data from JENDL-5, ENDF/B-VIII.0 and JEFF-3.3 libraries., the one-sigma (68.2%) and the two-sigma (95.4%) distributions of the neutrons are represented by the thick and thin x-axis bars, respectively.

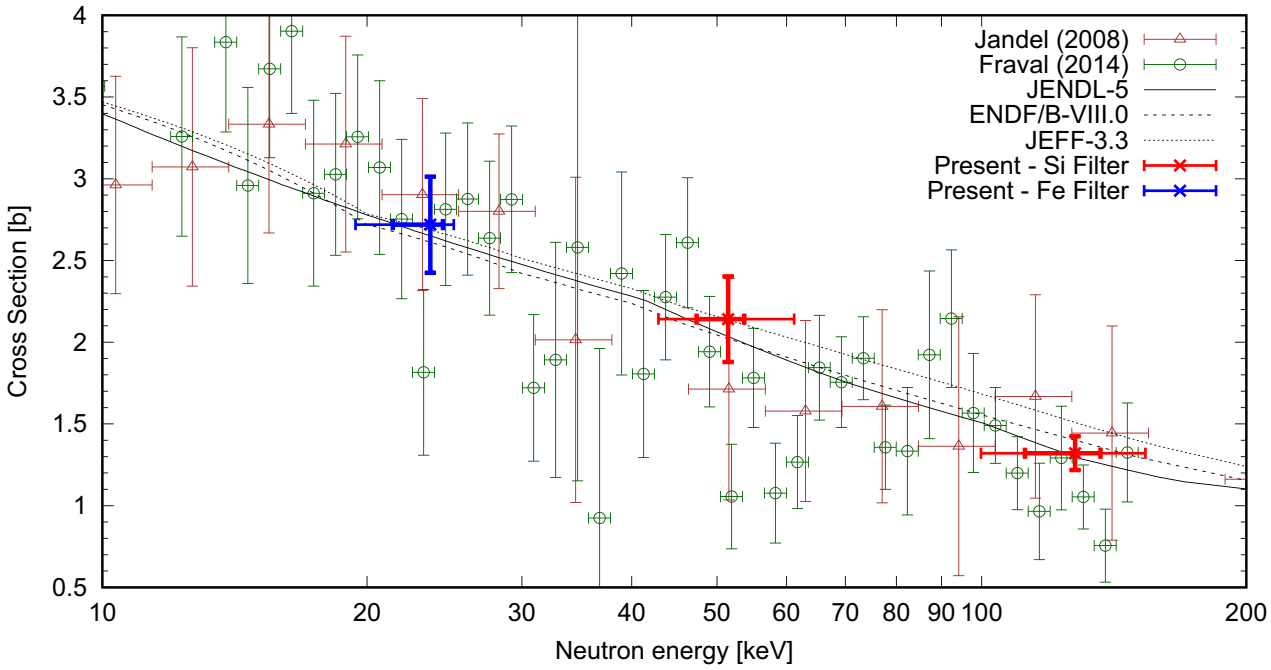

Figure 13. Neutron capture cross-section results for ^{241}Am compared to the latest experimental data and evaluated nuclear data from JENDL-5, ENDF/B-VIII.0, and JEFF-3.3 libraries in more detail. For the present results, the one-sigma (68.2%) and the two-sigma (95.4%) distributions of the neutrons are represented by the thick and thin x-axis bars, respectively.

Table 6. Summary of the ^{241}Am Cross-Section Results.

Filter element	Centroid Energ.[keV]	σ dist [keV]	2 σ dist [keV]	Cross-Section [b]	Uncertainty [b]
Fe	23.5	21.4–24.4	19.4–25.1	2.72	0.29
Si	51.5	42.9–61.2	47.4–53.7	2.14	0.26
	127.7	112.0–136.5	99.8–153.5	1.32	0.10

been considered in the cross-section calculation. The present results show agreement within uncertainties with the recommended values from JENDL-5, ENDF/B-VIII.0 and JEFF-3.3 and present much lower total uncertainties than the experimental data from Jandel *et al.* and Fraval *et al* that present uncertainties in the keV region over 20 keV over 20%.

Moreover, since the present ^{241}Am neutron capture cross-section results were obtained relative to the measured ^{197}Au neutron capture yield, the ^{197}Au neutron capture cross-section was determined using the energy dependence of the neutron flux derived from the boron measurement. Typical time-of-flight experiments usually rely on the energy dependence of the neutron flux, commonly determined using a boron sample, that has to be normalized. However, in the present experimental setup, due to the use of the neutron filtering system, a complementary measurement without the use of the filter material is required in order to normalize the incident neutron flux to the saturated first resonance of ^{197}Au, which might hamper the accuracy of the measurement. Hence, it was decided the rely on the ^{197}Au neutron capture yield as no normalization is required due to the pulse-height weighting technique. Notwithstanding, the energy dependence of the neutron flux measured with the boron sample was determined using this methodology in order to evaluate the accuracy of the ^{197}Au neutron capture yield by means of determining the ^{197}Au neutron capture cross-section. The ^{197}Au neutron capture cross-section are shown in Figure 14 measured at the same energies of 23.5, 51.5 and 127.7 keV with good agreement within uncertainties with both evaluated and experimental data that validates the accuracy of the ^{197}Au neutron capture yield.

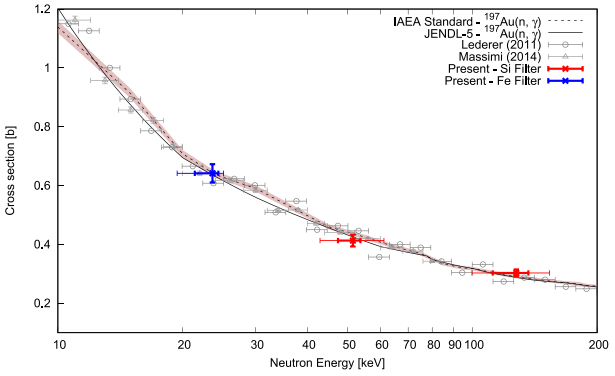

Figure 14. Neutron capture cross-section results for ^{197}Au compared to the latest experimental data and evaluated nuclear data from JENDL-5 and the standard IAEA libraries. For the present results, the one-sigma (68.2%) and the two-sigma (95.4%) distributions of the neutrons are represented by the thick and thin x-axis bars, respectively.

5. Conclusions

The neutron capture cross-section of ^{241}Am was measured in the ANNRI beamline of the MLF facility at J-PARC at the neutron incident energies of 23.5, 51.5, and 127.7 keV. In order to bypass the effect of the double-bunch mode of J-PARC, the newly developed neutron filtering system of the ANNRI beamline was employed using filter configurations of 20 cm of ^{nat}Fe and ^{nat}Si in separate measurements. In the present work, the ^{241}Am neutron capture cross-section was measured to be 2.72(29) b at 23.5 keV, 2.14(26) b at 51.5 keV and 1.32(10) b at 127.7 keV. The present results provide much higher accuracy, in terms of lower total uncertainties, than any of the latest available time-of-flight experimental data sets over 20 keV. The present results are important in order to reduce the influence of the nuclear data uncertainty in the design of ADS facilities, as the current results display uncertainties from 8 to 12% compared to the uncertainties of around 20% present in the latest results of Jandel *et al.* and Fraval *et al.* Moreover, the JENDL-5, ENDF/B-VIII.0 and JEFF-3.3 evaluated nuclear data libraries are able to reproduce the present results within uncertainties, except for the result at 127.7 keV, where the JEFF-3.3 library overestimates the present results.

Acknowledgments

The neutron experiments at the MLF of the J-PARC were performed under the user program (Proposal 2021P0301).

Disclosure statement

No potential conflict of interest was reported by the author(s).

ORCID

Gerard Rovira http://orcid.org/0000-0002-3031-6204

References

[1] Annual Report 2020. [Internet]. GEN-IV International forum; [Released in Jun 2021; cited 2021; cited 20 Dec 2021 Jun 2021; cited 20 Dec 20]. Available from: https://www.gen–4.org/gif/jcms/c178290/gif–2020–annual–report

[2] Pyeon CH, Yamanaka M, Oizumi A, et al. First nuclear transmutation of ^{237}Np and ^{241}Am by accelerator-driven system at Kyoto university critical assembly. J Nucl Sci Technol. 2019;56(8):684–689.

[3] Tsujimoto K, Sasa T, Nishihara K, et al. Neutronics Design for Lead-Bismuth Cooled Accelerator-Driven System for Transmutation of Minor Actinide. J Nucl Sci Technol. 2004;46(8):812–822.

[4] Sugawara T, Takei H, Iwamoto H, et al. Research and development activities for accelerator-driven system in JAEA. Progress in Nuclear Energy. 2018;106:27–33.

[5] Sugawara T, Katano R, Tsujimoto K, et al. Impact of impurity in transmutation cycle of neutronics design of revised accelerator-driven system. An Nucl Energ. 2018;111:449–459.

[6] Shibata K, IWAMOTO O, Nakagawa T, et al. JENDL-4.0: a new library for nuclear science and engineering. J Nucl Sci Technol. 2011;48:1–30.

[7] Iwamoto H, Nishihara K, Sugawara T, et al. Sensitivity and uncertainty analysis for a minor-actinide transmuter with JENDL-4.0. Nucl Data Sheets. 2014 April;118:519–522.

[8] Iwamoto H, Nishihara K, Sugawara T, et al. Sensitivity and uncertainty analysis for an accelerator-driven system with JENDL-4.0. J Nucl Sci Technol. 2013;50(8):856–862.

[9] JENDL-5.0 [Internet]. nuclear data center, japan atomic energy Agency. cited 2022 Jan 12]. Available from 2022 Jan 12: https://wwwndc.jaea.go.jp/jendl/j5/j5.html

[10] Fraval K, Gunsing F, Altstadt S, et al. Measurement and analysis of the ^{241}Am(n,γ) cross section with liquid scintillator detectors using time-of-flight spectroscopy at the n_TOF facility at CERN. Phys Rev C. 2014;89:044609.

[11] Jandel M, Bredeweg TA, Bond EM, et al. Neutron capture cross section of ^{241}Am. Phys Rev C. 2008;78:034609.

[12] V1720 8 channel 12 bit 250 MS/s digitizer [Internet]. CAEN. cited 2022 Jan 12]. Available from 2022 Jan 12: https://www.caen.it/products/v1720/

[13] Rovira G, Kimura A, Nakamura S, et al. Neutron beam filter system for fast neutron cross-section measurement at the ANNRI beamline of MLF/J-PARC. Nucl Instrum Methods Phys Res. 2021; 1003:165318.

[14] Rovira G, Kimura A, Nakamura S, et al. KeV-neutron capture cross-section measurement of ^{197}Au with a Cr-filtered neutron beam at the ANNRI beamline of MLF/J-PARC. J Nucl Sci Technol. 2022;59(5):647–655.

[15] Kodama Y, Katabuchi T, Rovira G, et al. Measurements of the neutron capture cross section of ^{243}Am around 23.5 keV. J Nucl Sci Technol. 2022;58(11):1159–1164.

[16] Terada K, Kimura A, Nakao T, et al. Measurements of neutron total and capture cross sections of ^{241}Am with ANNRI at J-PARC. J Nucl Sci Technol. 2018;55(10):1198–1211.

[17] Harada H, Iwamoto O, Iwamoto N, et al. Research and development for accuracy improvement of neutron nuclear data on minor actinides. EPJ Web of Conferences. ND 2016: International Conference on Nuclear Data for Science and Technology 11 - 16 Sep 2016 Bruges, Belgium, 2017; 146:11001.

[18] Sato T, Iwamoto Y, Hashimoto S, et al. Features of particle and heavy ion transport code system PHITS version 3.02. J Nucl Sci Technol. 2018;55:684–690.

[19] Macklin, Macklin RL, Gibbons JH, et al. Capture-cross-section studies for 30-220 keV neutrons using a new technique. Phys Rev. 1967;159:1007–1015.

[20] Moxon MC, Rae ER, et al. A gamma-ray detector for neutron capture cross-section measurements. Nucl Inst Meth. 1963;24:445–455.

[21] Ohsaki T, Nagai Y, Igashira M, et al. An NaI(Tl) spectrometer system for keV neutron radiative-capture reactions. Nuc Ins Meth Phys. 1999;A425:302–319.

[22] Verbeke JM, Hagmann C, Wright D, et al. Simulation of neutron and gamma ray emission from fission and

photofission. Lawrence Livermore National Laboratory; 2016. UCRL-AR-228518-REV-1

[23] Iwamoto O, Iwamoto N, Kunieda S, et al. The CCONE code system and its application to nuclear data evaluation for fission and other reactions. Nucl Data Sheets. 2016;131:259–288.

[24] Rovira G, Katabuchi T, Tosaka K, et al. KeV-region analysis of the neutron capture cross-section of ^{237}Np. J Nucl Sci Technol. 2022;59:110–122.

[25] Carlson AD, Pronyaev VG, Capote R, et al. Evaluation of the neutron data standards. Nucl Data Sheets. 2018;148:143–188.

[26] Brown DA, Chadwick MD, Capote R, et al. ENDF/B-VIII.0: the 8th major release of the nuclear reaction data library with CIELO-project cross sections, new standards and thermal scattering data. Nucl Data Sheets. 2018;149:1–142.

[27] Kellet MA, Bersillon O, et al. The decay data evaluation project (DDEP) and the JEFF-3.3 radioactive decay data library: combining international collaborative efforts of evaluated decay data. EPJ Web of Conferences. ND 2016: International Conference on Nuclear Data for Science and Technology 11-16 Sep 2016 Bruges, Belgium. 2017;146:02009.